ORIGINAL ARTICLE

lajss.org
Latin American Journal of Solids and Structures

www.lajss.org

Dispersion Properties of Fragments of Square Metal Shells Driven by Explosive Loading

Xinyue Huang[a], Yufei Zhang[b], Han Liu[a]*, Zhiwei Guo[a]*, Anhong Chen[b], Guangyan Huang[a]

[a]State Key Laboratory of Explosion Science and Technology, Beijing Institute of Technology; Beijing 100081, P. R. China. Email: 1411897448@qq.com, liuh@bit.edu.cn, guozwbit@bit.edu.cn, huanggy@bit.edu.cn

[b]Science and Technology on Space Physics Laboratory, China Academy of Launch Vehicle Technology, Beijing 100076, China. Email: zhangyf_2016@126.com, Achen@163.com

* Corresponding author

https://doi.org/10.1590/1679-78257833

Abstract

The fragment dispersion properties of metal shells under internal explosive loading are important topics in the fields of public safety and defence technology. The internal explosion driving phenomenon of square charge structures is common in the design of innovative warheads, the protection of improvised explosive devices (IEDs), the storage of hazardous materials, etc., and it is essential to investigate their fragment dispersion characteristics. In this study, the effect of the eccentric initiation on the circumferential fragment speed of the square charge structure was investigated via high-speed impulse X-ray experimental technique and numerical simulating methods. Furthermore, a high-order polynomial calculation formula for the circumferential fragment dispersion speed of the square charge structure under different eccentric coefficients for initiation was established based on the numerical and experimental data. The results of this study would provide references for the disposal of IEDs and the design of warheads.

Keywords

pulse X-ray photography; square charge structure; fragment speed; eccentric initiation

Graphical Abstract

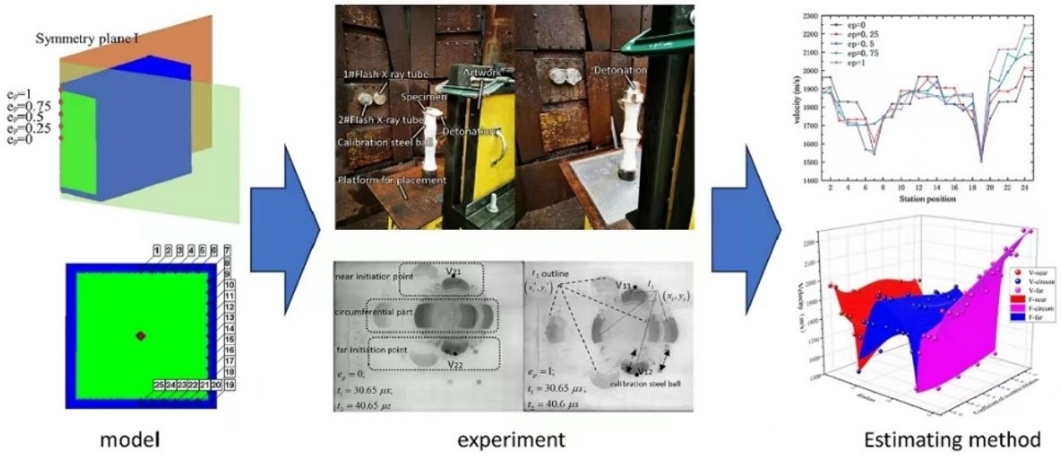

Received: September 13, 2023. In revised form: September 14, 2023. Accepted: September 21, 2023. Available online: September 29, 2023
https://doi.org/10.1590/1679-78257833

1 INTRODUCTION

Under the action of explosive loading of internal explosives, expansion, breaking, dispersion, and other phenomena occur in metal shells, which are common when warheads explode and are damaged, improvised explosive devices (IEDs) pose threats and other scenes happen, and it is important to deeply research them for the development of defence technologies and public safety technologies. Most of traditional fragment warheads or improvised explosive devices are axisymmetric structures, whose initiation points are set in their rotational symmetry axes. When the charges inside warheads explode, the metal shells or prefabricated fragments of warheads quickly accelerate under the drive of expansion of explosive detonation products, producing numerous high-speed fragments that impact penetration targets, causing damage. However, in recent years, the internal explosion drive problem of non-axisymmetric shells has emerged as a research hotspot in the fields of warhead technology and explosion protection, and special-shaped shell structures, e.g. polygonal-prism, D-shaped, and oval fragment structures, have attracted considerable attention from researchers worldwide.

Owing to the increasing demand for advanced combat platforms for efficient and accurate damage, various directional and efficient damage technologies have been developed [1]. The polygonal-prism charge structure can produce one to several directional enhanced damage directions [2]. D-shaped charge refers to the charge structure whose cross section has the shape of the letter 'D', which can achieve a higher gain of damage energy in the aim direction through the optimisation of the structural design and initiation mode [3]. Deng et al. found that an oval charge structure had a fragment focusing effect in the direction of the minor axis of the oval [4]. As indicated by these studies, the occurrence scenes of the explosion damage and fragment dispersion property of non-axisymmetric shells have gradually become common. Additionally, as public safety technologies have increasing requirements for the accurate disposal capacity of explosives, the importance of researchers' ability to accurately analyse the damage and threat of explosive fragments is increasing. The explosion damage fields of charge structures with different shapes, length–diameter ratios, shell materials, and explosive varieties have visible differences, which are essential for the design and strength enhancement of explosion protection structures. In summary, it is becoming increasingly important to research non-axisymmetric charge structures.

The breaking and fragment dispersion effects of metal shells under the action of internal explosion have been researched for a long time, and relevant studies are abundant. For example, studies have focused on an infinitely long cylinder charge, a finitely long cylinder charge, and other relatively ideal axisymmetric structures with central initiation, along with D-shaped charge, prismatic non-axisymmetric charge, and other irregular working conditions with non-central initiation. With regard to axisymmetric fragment structures, the Gurney formula is a typical fragment dispersion speed calculation method [5]; however, it does not consider the rarefaction wave effect at the end of the warhead, under the assumption of an infinitely long charge. Thus, Gao et al. analysed the influence of the rarefaction wave on the fragment acceleration process and proposed a formula for predicting the speed distribution [6]. Liao et al. proposed a fragment speed distribution formula for a finitely long cylindrical shell charge with an end cover [7]. Furthermore, for the eccentric initiation phenomenon, Lv et al analysed the fragment speed field of directional warheads with eccentric initiation; the results suggested that the fragments in the opposite direction of the initiation point had the highest dispersion speed, and the gain reached 10.45% [8]. Li calculated the speeds of fragments near and on the opposite side of the initiation point during eccentric two-line initiation [9–11] according to one-dimensional detonation drive theory. Wang et al. proposed a formula considering the charge–weight ratio, charge diameter, axial sparse effect, and eccentric initiation to predict the dispersion direction angles of charge shell fragments during one-end initiation [12].

In summary, there have been numerous studies on the distribution properties of the fragment speed of axisymmetric warheads with traditional rotational bodies and the influence rule on the eccentric initiation, and accurate empirical formulas and numerical calculation models have been established for calculating the fragment speed distribution properties [13]. Moreover, researchers have studied the fragment speed distribution of typical non-axisymmetric warheads and the effects of different eccentric initiations [2,14-15], and relevant research results have satisfied the analysis requirements for the corresponding explosion fragment strength to some extent.

However, there are relatively few studies and reports on calculation models for the fragment dispersion properties of prismatic charge structures—particularly square charge structures—and the change rule under the action of eccentric initiation. In addition, owing to the shortage of analysis of the dynamic response of square shells under the action of internal explosive loading and the formation process of the strength field properties, researchers' ability to design new irrotational body warheads and engineer special-shaped explosive disposal is limited. It is important to analyse the shell movement, breaking, and dispersion properties of square metal shells under the action of internal explosion of explosives. In this study, a typical square charge structure was designed for analysing the dynamic response and fragment dispersion properties of square metal shells under the action of internal explosion. A high-speed pulse X-ray photography experiment and numerical simulations based on smoothed-particle hydrodynamics (SPH) were performed, and a

calculation model for the fragment dispersion speed of a square charge structure under different initiation statuses was established. This study lays a theoretical foundation and provides engineering application reference for the design of square fragment warheads and explosion protection structures.

2 Internal Explosion Drive Experiment of Square Metal Shells

2.1 Design of High-speed Pulse X-ray Static Explosion Experiment

Pulse X-ray photography is widely used in the relevant studies during the process of testing the explosive loading responses of metal shells, and it measures the change rule of the internal part during the rapid reaction process by virtue of the penetration capacity of X-rays. X-ray high-speed photography technology is applicable to high-speed reaction processes that tend to produce intense incandescent light, dispersed material particles, dense smoke, dust, or particle clouds that prevent the visible light from capturing the ontology of the substance under test. As an important experimental technology in the fields of terminal ballistics and explosion research, X-rays are also applicable to photographing metallic and non-metallic shields and have been widely used in the study of ballistics, explosion mechanics, high-speed collisions, plasma, and other action processes [16].

Figure 1 shows a schematic of the square charge structure considered in this study. The charge structure has a square cross section with side length a and shell thickness h in the direction of the main charge shape edge normal direction, and it is internally charged with the explosive Comp. B. Owing to the protection requirements of the high-speed pulse X-ray photography device for explosion fragments, an end cover is not installed at the end of the charge structure [7]. Then, owing to the need to counteract the effects of rarefaction waves at the end [17-19], the length–diameter ratio of the charge structure needs to be significantly larger than 2 while the design parameter system to enable a square charge structure is considered: the internal square charge has a side length of 35 mm, the axial length of the charge part L is 100 mm, and the shell thickness h is 2 mm. With these parameters, the length–diameter ratio of the charge structure is approximately 2.86, which satisfies the requirement of the charge structure without an end cover. Additionally, the total charge mass is approximately 422.69 g, which satisfies the requirement of the pulse X-ray testing device for safety protection. The parameters of the charge structure are shown in Table 1.

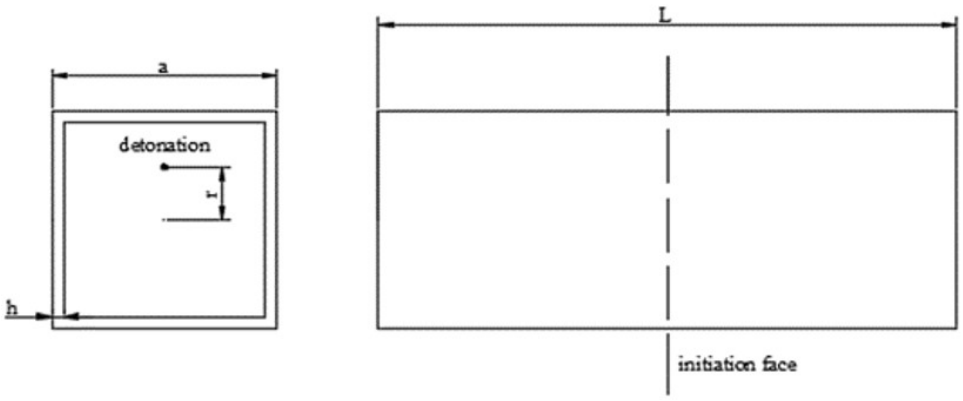

Figure 1. *Schematic of the square charge structure.*

Table 1. Dimensions of the square charge structure.

Length of casing (L,mm)	Side length of shell (a,mm)	Thickness of side of column (h,mm)	Density of shell (ρ_m,kg/ m^3)	Density of Comp. B (ρ_c,kg/ m^3)
100	39	22	7.85	1.717

The square charge structure does not have rotational symmetry; thus, its eccentric initiation effects are more complex than those of the cylinder charge structure. Therefore, to initially analyse its eccentric initiation effects, we mainly examined the situation where the initiation point is on the symmetry axis. On this premise, we studied the square charge structure fragment dispersion properties under two initiation methods: end centre initiation and centre section endpoint initiation. The initiation points are shown in Figure 2.

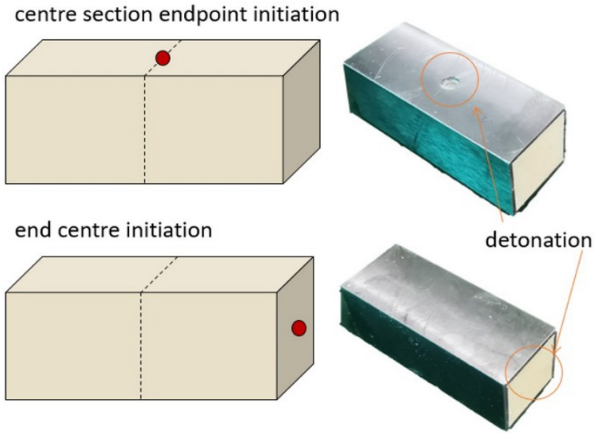

Figure 2. *Schematic of the initiation points.*

To test the typical moment and fragment dispersion speed properties of the square charge structure during the explosion drive process, the parallel high-speed pulse radiography method was used. Figure 3 shows a schematic of the high-speed photography device setup. Two ray tubes were used to capture successive dynamic images at different moments (t1 and t2) immediately after the initial speed was reached. Two images were formed on the same negative film, and a computerised image processing system was used to scan the shell X-ray images for identification, providing the basis for establishing the coordinate system and acquiring the observation points.

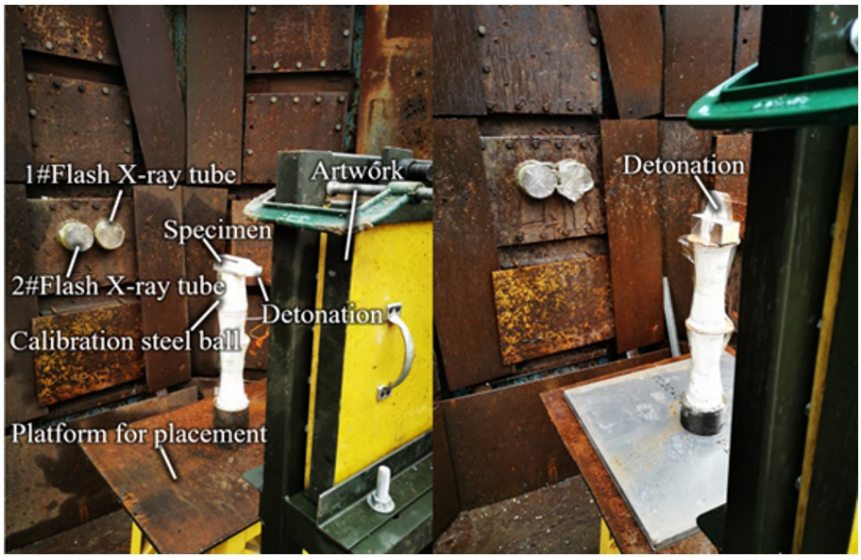

Figure 3. *High-speed pulse X-ray test devices (left: end centre initiation; right: centre section endpoint initiation).*

2.2 High-speed Pulse X-ray Experiment Results

The pulse X-ray images of the square charge structure with two initiation methods under the action of internal explosion of explosives during the fragment dispersion process are presented in Figure 4. As shown, under the two initiation methods, the square charge structure was divided into four areas, that is, the areas where the four sides were located. For the eccentric initiation status, according to the surface symmetry of the square charge structure, it was divided into three parts: the near initiation end, circumferential part, and far-from- initiation end.

According to the shape of shell expansion, these three parts of the shell were dispersed in an arc, and the dispersion speed of the shell in the middle area was the highest. This is explained as follows: with the release of explosive implosion energy, shell breakage at right-angle turns caused rarefaction wave transmission, dispersing the energy, but the middle shell was less affected by the rarefaction wave than the other parts; thus, the response part had the highest speed, causing the shell to expand faster and eventually disperse in a convex shape.

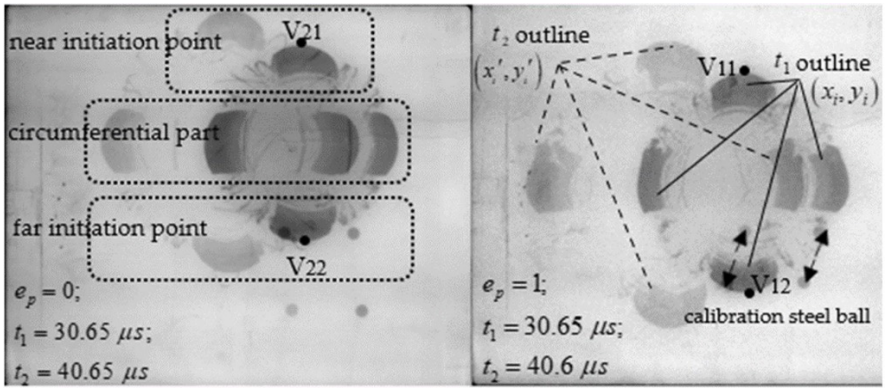

Figure 4. *Left: centre section endpoint initiation; right: shell dispersion under end centre initiation.*

The fragment speed of the charge structure was analysed, as shown in Figure 4. The diameter of the locking ball and the coordinates of its centre were recorded in the software system. The coordinate system at different moments was determined according to the circle centre of the locking ball at different moments, and the unit length of the coordinate system was determined with consideration of the steel ball diameter of 8 mm. Thus, the coordinates (xi, yi) and (x`i, y'i) of the near initiation point and far initiation point, respectively, at the centre section under different initiation methods were acquired. The speed of each tested point was determined using the following formula:

$$v_i = \frac{\sqrt{(x_i - x_i')^2 + (y_i - y_i')^2}}{\triangle t} \tag{1}$$

where Δ*t* represents the time interval between two pulse X-rays.

According to the processing method for the initiation speed described above, speed test results were obtained from the X-ray test and simulation of static explosion under two different initiation methods of the square charge structure: for the square charge structure with centre initiation, the fragment initiation speeds of the charge structure on the initiation side and non-initiation side were V_{11} = 2017.64 m/s and V_{12} = 1897.13 m/s; for the charge structure with eccentric initiation, its speeds on the initiation side and non-initiation side were V_{21} = 1916.8 m/s and V_{22} = 2324.65 m/s, respectively.

3 Numerical Calculation of Metal Shell During Internal Explosion Drive Process

3.1 Problem Description

Only the shell drive status and fragment dispersion forms at particular moments can be observed in the high-speed pulse X-ray experiment; thus, the force–moment curve of the shell cannot be analysed. Meanwhile, owing to the high cost and complexity of the high-speed pulse X-ray experiment, there is no way to experimentally research multiple operating conditions. Therefore, to study the influence of different eccentric effect initiations on the circumferential fragment speed of the square charge centre section, we used Ansys Autodyn for the numerical analysis of the dispersion mechanism of the square charge structure warhead under the action of internal explosion and established a numerical analysis model of the square charge structure under different initiation points, to study the changes in the fragment speeds of internal explosion under different initiation statuses.

3.2 Material Model

The square charge structure considered in this study has two main materials in the dynamic response process under internal explosive loading: ① the metal shell and ② the charge explosive. The Johnson–Cook (JC) model was utilised to describe the deformation and damage at high strain rates for AISI 1045—the material used for the warhead:

$$\sigma = （A + B\varepsilon_{\mathrm{ep}}^{n})(1 + C\ln\dot{\varepsilon}^{*})(1 - T^{*m}） \tag{2}$$

where *A* represents the yield strength; *B* is the strain strengthening factor; *C* is the strain-rate strengthening factor; *m* and *n* are the softening and strain strengthening factors, respectively; ε_{ep} represents the equivalent plastic strain; , with

being the plastic strain rate; $\dot{\varepsilon}_0 = 1.00s^{-1}$ represents the reference strain rate; and $T^* = (T–T_r)/(T_m–T_r)$, with T_r = 293 K being the indoor temperature and T_m being the melting temperature. The parameters of AISI 1045 are shown in Table 2.

Table 2. JC parameters of AISI 1045 steel.

Material	A (MPa)	B (MPa)	C	m	n	Tm (K)
AISI 1045	507	320	0.064	1.06	0.28	1793

The Jones–Wilkins–Lee equation of state was used to describe the mechanical behaviour of the detonation products generated after initiation for explosive B filled inside the metal shell:

$$p_e = C_1(1-\frac{\omega}{R_1V})e^{-R_1V} + C_2(1-\frac{\omega}{R_2V})e^{-R_2V} + \frac{\omega E}{V} \tag{3}$$

where p_e represents the pressure of the detonation products, E represents the volumetric internal energy, V represents the initial relative volume, and C_1, C_2, R_1, R_2, and ω are material property parameters. The parameters of Comp. B are shown in Table 3.

Table 3. Properties and parameters of Comp. B.

Material	Density r (kg/m^3)	Detonation velocity D (m/s)	C-J pressure (GPa)	C_1 (GPa)	C_2 (GPa)	R_1	R_2	ω
Comp. B	1.717	7980	29	524	768	4.2	1.1	0.34

3.3 Calculation Method

SPH is a non-grid computing method that has gradually been developed over the past >20 years. It describes materials as interacting particles with various physical properties, such as mass, pressure, and speed. The dynamic behaviours can be solved by solving the kinetic equation of the particles and tracing the motion of each particle. The dynamic response of the charge structure under the action of explosion and the process of shell breaking are often related to high speeds, large strains, and severe material breaking. As a non-grid method, SPH can avoid the problems of excessive grid deformation and difficult failure criteria setting caused by explosion in the traditional grid-based calculation methods and also avoid the difficulty of capturing the material interface using the Euler method. Therefore, in this study, the dynamic response of the charge structure under eccentric initiation and the process of shell breaking were studied via SPH numerical simulation.

The SPH method requires a large number of homogeneous particles to ensure the accuracy of the simulation calculation. A smaller particle diameter corresponds to a higher calculation accuracy; however, an excessively small particle diameter will lead to time-consuming model computations; thus, a suitable particle diameter must be selected. The minimum fragment in Autodyn needs to consist of at least two particles, and the minimum fragment length in this model was 2 mm. To improve the readability of the data in the fragmented shell, six different sets of particle diameters were established in this study: 1, 0.6, 0.5, 0.4, 0.3, and 0.2 mm. The relative error was obtained by comparing the maximum initial speed reached by the fragments with experimental data, as shown in Figure 5. When the particle diameter was <0.6 mm, the error of the simulation data relative to the experimental data was nearly within 5%, and the results of a previous study [20] also show that the particle diameter of 0.4 mm is suitable with regard to the accuracy of the results and the calculation efficiency. According to the results, this numerical model with SPH particle size set to 0.4 mm can reliably predict the fragment speed distribution of the centre section of the square charge structure under end centre initiation and centre section endpoint initiation.

According to the structure sizes presented in Section 2.1 and the material model presented in Section 3.2, the shell breaking and dispersion properties of the square charge structure described in Section 2.1 during the end centre initiation of the charge structure under the action of the internal implosion of explosives were compared with the results of the high-speed pulse X-ray experiment, as shown in Figure 6. The shell dispersion forms in the SPH numerical simulation results agreed well with the shell profile forms obtained via high-speed pulse X-rays. The vertical dispersion fragment speed of the charge structure, measured by Gauges, is 2070.71 m/s, which has a relative error of 2.63% from the X-ray experimental results. Therefore, it can be considered that the particle size of 0.4 mm can satisfy the analysis requirements for the fragment dispersion properties.

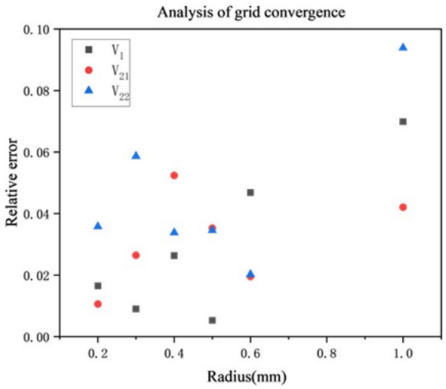

Figure 5. Analysis of grid convergence.

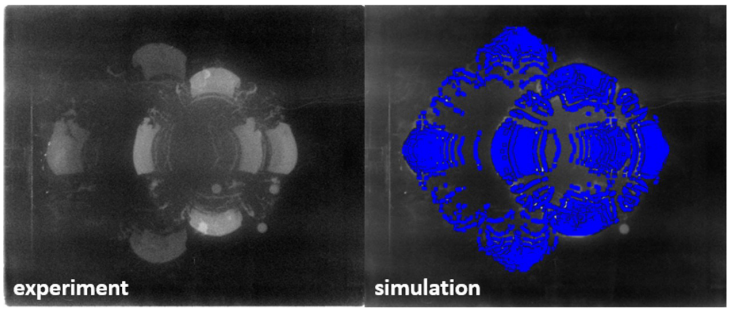

Figure 6. Contrast between experimental results and numerical calculation results.

3.4 Numerical Model

3.4.1 Eccentric Initiation Model

The square warhead structure studied in this section is the same as the centre section endpoint initiation described above, which is mainly divided into the explosives and shell. The initiation point of the warhead was set at different distances (*r*) from the centre section to the centre point, which was represented by the eccentricity coefficient $e_p = 2r/a$. According to the symmetry of the warhead, the internally charged explosives, and the detonation point, the cost of operation can be reduced by building a quarter model.

As shown in Figure 7, the shell model is consistent with the experimental part above and is distributed axially and axisymmetrically; thus, only half of it needs to be considered, and the axisymmetric situation of the initiation point is mainly discussed. On this premise, to study the effects of different initiation positions on the particle speed of the middle end shell, with the centre of the square charge section as the reference point, the ratio of the distance from the initiation point to the base point to the distance from the centre of the charge structure to the edge is taken as the eccentric initiation coefficient of the charge structure (i.e. the parameter e_p in the figure), which ranges from 0 to 1. By using the numerical simulation experiment of the square charge structure of the centre initiation as a control group, the effects of eccentric initiation on the shell breaking and particle dispersion speed were studied comparatively. According to the centre line of square charge structure shape, we set the angle between the connection of the observation point and the centre and the symmetry plane I to ϑ. According to the symmetry of the warhead with a square charge structure, a numerical calculation model, as shown in the figure, is established to indicate the shell position as (e_p,ϑ).

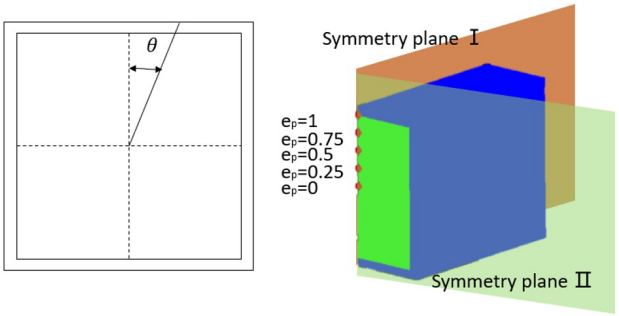

Figure 7. Positions of test points under different eccentricity coefficients.

3.4.2 Dynamic Response Process of Warhead Under Internal Explosive loading

To illustrate the shell breaking process of the warhead under the eccentric initiation factors e_p = 0 and e_p = 1, Figure 8 presents the material position and pressure cloud charts of the square charge structure at different moments under the two initiation methods.

According to the rarefaction wave propagation, the initiation point was in the junction of shell and the explosives when the eccentricity coefficient was 1, the shell began to break at the time of initiation, and the rarefaction waves in the fragment end reduced the detonation wave pressure within the explosives. As shown in the figure, the strength of the detonation waves when the eccentricity coefficient was 1 was significantly lower than that during centre initiation, and owing to the difference in initiation positions, the particles of the non-initiation plane began to accelerate earlier in the former case.

According to the breaking of the warhead shell, the particle dispersion time of the initiation end when the eccentricity coefficient was 1 was smaller than that during centre initiation, and the shell breaking degree was larger than that of the non-initiation end. The shell breaking degree and shell dispersion degree during centre initiation exhibited the property of central symmetry. The structure of the square warhead at right angles was the first to break and had the lowest particle dispersion speed. The breaking degrees of the initiation end and non-initiation end were not evenly distributed, and when the eccentricity coefficient was not 0, the shell at the initiation end broke earlier than that at the non-initiation end.

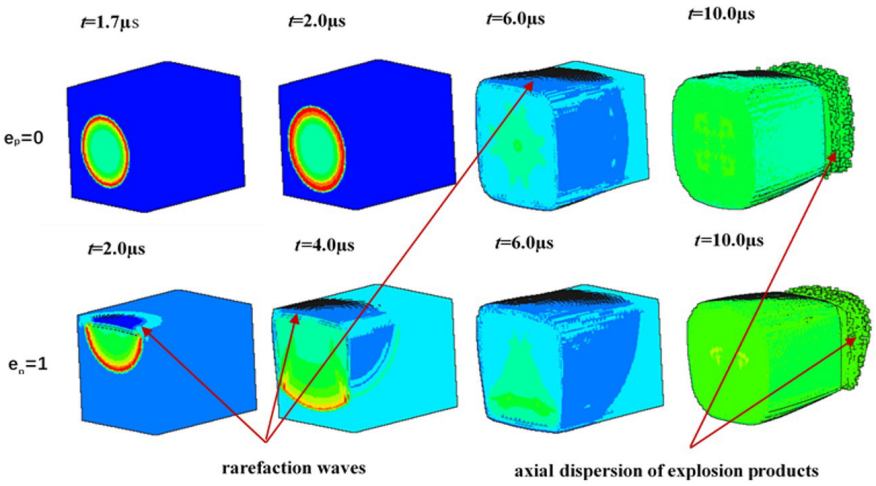

Figure 8. Propagation process of detonation waves in the square charge structure with eccentricity coefficients of e_p = 0 and e_p = 1.

3.4.3 Fragment Speed Contrast of Warhead

The fragment dispersion speed of the warhead is one of the important parameters in the design of the warhead, and the fragment must carry enough kinetic energy to puncture the protective structure of the target. To examine the gain effect of the eccentricity initiation on the fragment speed, the circumferential fragment speed of the centre section of the square charge structure examined in this study was analysed according to the numerical calculation results. Figure 9 shows a schematic of the test points set in the numerical simulation and the speed of each test point of initiation under different eccentricity coefficients; each test point is located in the middle of the shell. Overall, it can be seen that regardless of the magnitude of the eccentricity coefficient, the lowest particle speed at the right angle of the square shell correlated to shell breaking discussed above, which is due to the stress concentration phenomenon resulting from large changes in shell shape. The fragment speeds at the initiation and non-initiation ends were not evenly distributed; when the initiation end was closer to the initiation point, the Gauges number was smaller, and the fragment speed was higher. The opposite was true for the non-initiation end, because the pressure release at the right angle after the shell breaking caused the sparse wave to propagate inward, and a stronger sparse wave corresponded to a lower fragment speed.

As shown in Figure 9, during the centre initiation, the speeds of the initiation and non-initiation ends were axisymmetrically distributed, and the fragment speed was the highest near the initiation point. At the same test point, as the eccentricity coefficient increased, the fragment speed of the non-initiation end increased, and that of the initiation end decreased. The change was larger for the non-initiation end, with a range of –200 to 300 m/s and a speed gain of –9% to 10%. The speed distribution suggests that the fragment speed near the initiation end was slightly lower than that near the non-initiation end, which was because the eccentric initiation extended the distance from the detonation wave to the non-initiation end and provided more energy for the shell breaking at the non-initiation end, increasing the fragment speed of the shell. This trend is consistent with the findings of previous studies.

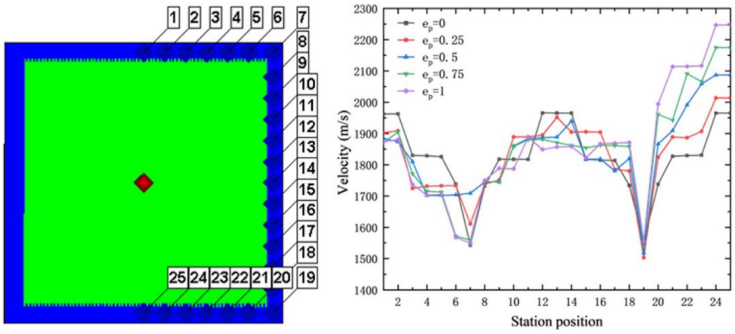

Figure 9. Schematic of test points.

Figure 10 presents the shell dispersion and breaking process at different moments under the eccentricity coefficients $e_p = 0$ and $e_p = 1$, showing the shell acceleration process of eccentric initiation for different parts of the square warhead. With $e_p = 0$, the shell evenly broke in the form of central symmetry. With $e_p = 1$, at t = 14 μs, the initiation end was dispersed relatively far. The non-initiation end was dispersed relatively far with $e_p = 1$ and t = 24 μs; the shell at the initiation end accelerated and broke first, and that at the non-initiation end accelerated later but was dispersed faster. The shell breaking degree of the initiation end exceeded that of the non-initiation end, which is consistent with the aforementioned results.

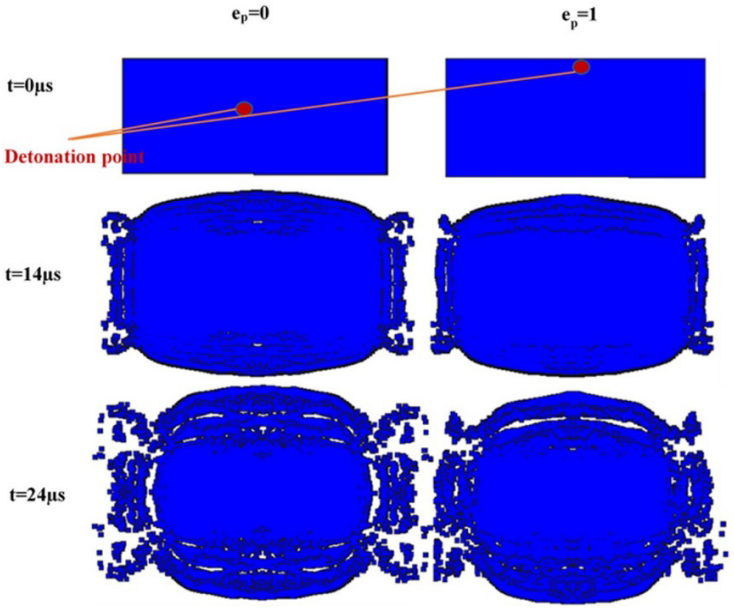

Figure 10. Contrast of shell dispersion and breaking with $e_p = 0$ and $e_p = 1$.

4 Segmental Fitting of Speed Formula

Explosive charges exploded to produce high-temperature and high-pressure detonation products, detonation products forced the shell to expand outward, the shell cracked when it expanded to certain degree, and cracks penetrated each other before forming fragments. The fragments began to move under the impact of detonation products, and their speed was called the initial speed. The initial speed of explosion fragments is an important parameter for measuring the cast distance of fragments and their target damage effect. It affects not only the dispersion range of fragments but also the potential degree of damage to surrounding facilities, equipment, and personnel. Gurney [5] proposed empirical formulas for the initial speed of predicted explosion fragments for different warheads shapes. For a cylindrical shell,

$$v_0 = \sqrt{2E_g}\sqrt{\frac{\beta}{1+0.5\beta}} \tag{4}$$

where $\sqrt{2E_g}$ is a Gurney constant (Gurney reported a linear relationship between $\sqrt{2E_g}$ and the detonation speed *D*, i.e. $\sqrt{2E_g} = 520 + 0.28D$, and $\beta = m_e/M$ is the ratio of the solid explosive mass m_e to the shell mass *M*. Huang et al. [13] obtained the axial velocity distributions of fragments when the eccentricity ratio was 0, 0.5, and 1 via high-speed pulse X-ray photography experiments for a short cylindrical charge structure with finite length and established an empirical formula for the axial distribution of fragment speed based on the experimental data matched with the initial eccentricity ratio and coefficient of the circular angle, whose form is as follows:

$$v_f = \sqrt{2E}\sqrt{\frac{f(a,\theta)\beta}{1+0.5f(a,\theta)\beta}} \tag{5}$$

where *f* is the modified factor of the eccentric initiation effect, which can be expressed as

$$f(a,\theta) = \begin{cases} \left(1-b_1 a^{b_2}\right)\left[1+b_3\left(1-\theta/\pi\right)a^{b_4}\exp\left(b_5\lambda\right)\right], a\in[0,0.5] \\ \left(1-b_6 a^{b_7}\right)\left[1+b_8\left(1-\theta/\pi\right)a^{b_9}\exp\left(b_{10}\lambda\right)\right], a\in[0,0.5] \end{cases} \tag{6}$$

Here,

$$\lambda = \sqrt{4a\cos^2\left(\theta/2\right)+\left(1-a\right)^2} \tag{7}$$

and b_1 to b_{10} are 10 empirical model parameters fitted from experimental data.

Li et al. [9] derived the partial differential governing equation of one-dimensional detonation wave load fragments based on the propagation rule of detonation waves, obtaining a semi-empirical formula for the radial speed distribution in the peripheral direction when the eccentricity ratio is 0–1. This formula is strictly closed; thus, it does not need experimental data fitted to formula parameters, and the distribution of fragment speeds can be calculated by determining the charge structure.

Through numerical simulations, we have investigated the circumferential velocity distribution of square charge structures under various eccentric initiation conditions. Taking into account the influences of different measurement point positions and initial eccentric detonation, we propose a velocity distribution formula, the fundamental polynomial form of which is as follows:

$$v_f(\theta,e_p) = \sqrt{2E_{\mathrm{g}}}\sqrt{\frac{\beta}{1+0.5\beta}} \bullet (a_{00}+a_{01}\cos\theta+a_{10}e_p+\ldots+a_{(n-1)1}\cos^{n-1}\theta\bullet e_p+a_{1(n-1)}\cos\theta\bullet e_p^{n-1}+a_{n0}\cos^n\theta+a_{0n}e_p^n) n=0、1、2\ldots \tag{8}$$

The correlation coefficient of the near initiation end and far initiation end was relatively high, and that of circumferential end was relatively low. The fragmentation resulting from shell strength leads to the homogenization of fragment velocities in the circumferential end region, resulting in a plateau phase of the velocity distribution and a reduced fitting degree. The fragment speeds of the shell of the square charge structure in the three areas were fitted. The most suitable orders and R^2 values of the square charge structure in the three areas are presented in Table 4.

Table 4. Polynomial orders and fitting degrees of the square charge structure in the three areas.

	Near initiation end	Circumferential end	Far initiation end
Order n	4	5	3
R^2	0.90039	0.77497	0.96857

Figure 11 shows a scatter diagram of the numerical calculation results and the high-order polynomial trend fitting chart, where red area is the near initiation end, the blue area is the circumferential end, and the purple area is the far

initiation end. As depicted in the figure, it can be observed that the scatter points in red and purple align with the regional trends of the computational formula, particularly in the proximity and distance from the initiation point where polynomial fitting yields satisfactory results. Nevertheless, due to the intricate interplay of shockwaves near the circumferential end and the partially homogenized nature of fragment velocity variations, the polynomial fitting outcomes in this area are comparatively more moderate. Despite this, these fitting results remain capable of providing reasonably accurate predictions of fragment velocity trends.

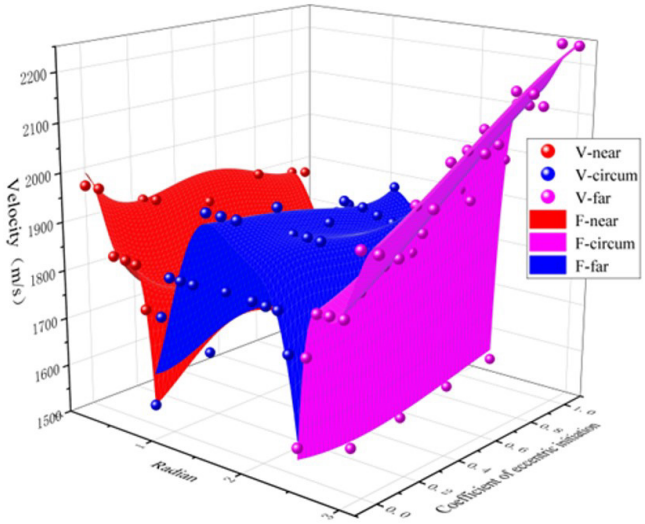

Figure 11. Scatter diagram of numerical calculation and the high-order polynomial trend chart.

5 Conclusions and Prospects

Experimental and numerical analyses were performed on the dynamic response and fragment dispersion properties of a square metal shell under the internal explosive loading of explosives. The effects of the eccentric initiation status on the fragment dispersion properties were analysed, and the empirical calculation formulas of the circumferential dispersion speed of fragments at the centre section were segmentally fitted. The following conclusions are drawn.

(1) Because the square metal shell has right-angle corners, the square metal shells considered in this study formed fewer small fragments under the internal explosion drive load of explosives compared with conventional axisymmetric charge structures, forming mainly four large fragments that dispersed in four areas overall.

(2) Under the eccentric initiation status, the shell fragment speed of the far initiation end had an overall increasing trend, while that of the near initiation end decreased significantly; thus, it can be initially considered that the eccentric detonation effect of square charge structures is essentially identical to that of axisymmetric charge structures.

(3) For the circumferential distribution properties of the fragment speed of the square charge structure, empirical formula fitting was performed for the dispersion speed of the near initiation end, lateral part, and far initiation end via the piecewise function fitting method. Overall, the fit was good. However, owing to the fragment pieces caused by shell strength, the dispersion speed of the circumferential end exhibited a plateau phase, and the fitting degree of the high-order formula was relatively low.

This study focused on the circumferential dispersion speed of the centre section of square charge structures. The changes in the axial fragment speed were not examined. In the future, these topics can be explored.

Author's Contribuitions: Conceptualization, Zhiwei Guo and Han Liu; methodology, Xinyue Huang and Yufei Zhang; software, Xinyue Huang; validation, Zhiwei Guo, Han Liu and Yufei Zhang; formal analysis, Xinyue Huang and Han Liu; investigation, Xinyue Huang; resources, Han Liu and Guangyan Huang; data curation, Han Liu; writing—original draft preparation, Xinyue Huang; writing—review and editing, Zhiwei Guo and Guangyan Huang; visualization, Xinyue Huang; supervision, Guangyan Huang; project administration, Guangyan Huang; funding acquisition, Guangyan Huang and Anhong Chen. All authors have read and agreed to the published version of the manuscript."

Editor: Marcílio Alves

References

1. Waggener, S. (2001). Relative performance of anti-air missile warheads. In *Proceedings of the 19th International Symposium of Ballistics, Interlaken, Switzerland* (pp. 623-630).

2. Ning, J., Duan, Y., Xu, X., & Ren, H. (2017). Velocity characteristics of fragments from prismatic casing under internal explosive loading. *International Journal of Impact Engineering, 109*, 29-38.

3. Guo, Z., Huang, G., Zhu, W., Liu, H., & Feng, S. (2019). Mechanism and Suppression of the Effect of Axial Rarefaction Waves on the Eccentric Initiation Effect. *International Journal of Impact Engineering, 124*, 37-47.

4. Deng, X., Wu, H., Yang, X., Xie, W., & Huang, F. (2022). Preformed Fragment Velocity Distribution of Elliptical Cross-section Projectile. *Latin American Journal of Solids and Structures, 19*(1), e423.

5. Gurney, R. W. (1943). The Initial Velocities of Fragments from Bombs, Shells, and Grenades. *Ballistic Research Laboratory (BRL) Report*.

6. Gao, Y., Zhang, B., Yan, X., Zhou, T., Xiao, X., & Feng, S. (2020). Axial Distribution of Fragment Velocities from Cylindrical Casing with Air Parts at Two Ends. *International Journal of Impact Engineering, 140*, 734-743.

7. Liao, W., Jiang, J., Men, J., Wang, S., Li, M., & Liu, H. (2021). Effect of the End Cap on the Fragment Velocity Distribution of a Cylindrical Cased Charge. *Defence Technology, 17*, 1052-1061.

8. Lv, S., Li, X., & Yang, Y. (2010). The Fragments Velocity and Destiny Distribution of the Eccentric Detonation Aimed Warhead. *Chinese Journal of Explosives & Propellants, 33*(5), 79-82.

9. Li, Y., & Wen, Y. (2017). Experiment and Numerical Modeling of Asymmetrically Initiated Hexagonal Prism Warhead. *Advances in Mechanical Engineering, 9*(1).

10. Li, Y., Li, Y., & Wen, Y. (2017). Radial Distribution of Fragment Velocity of Asymmetrically Initiated Warhead. *International Journal of Impact Engineering, 99*.

11. Li, Y., Li, X., Xiong, S., & Wen, Y. (2018). New Formula for Fragment Velocity in the Aiming Direction of an Asymmetrically Initiated Warhead. *Propellants, Explosives, Pyrotechnics, 43*(5), 496-505.

12. Wang, L., Han, F., & Zhou, Q. (2017). The Projection Angles of Fragments from a Cylindrical Casing Filled with Charge Initiated at One End. *International Journal of Impact Engineering, 103*, 138-148.

13. Huang, G., Li, W., & Feng, S. (2015). Fragment Velocity Distribution of Cylindrical Rings under Eccentric Point Initiation. *Propellants, Explosives, Pyrotechnics, 40*(2), 215-220.

14. Dhote, K., Murthy, K., Rajan, K., et al. (2015). Directional Warhead Design Methodology for a Tailored Fragment Beam. *Central European Journal of Energetic Materials, 12*(4), 637-649.

15. Ding, L., Li, Z., Liang, M., et al. (2017). The Dispersion Rule of Fragments about the Asymmetric Shell. *Shock and Vibration, 2017*, 9810978.

16. Ramudu, B. V., Reddy, C. J., & Madhu, V. (2019). Flash X-ray Radiography Technique to Study the High Velocity Impact of Soft Projectile on E-glass/epoxy Composite Material. *Defence Technology, 15*(2), 216-226.

17. Guo, Z.-W., Huang, G.-Y., Zhu, W., Liu, H., & Feng, S.-S. (2019). Mechanism and suppression of the effect of axial rarefaction waves on the eccentric initiation effect. *International Journal of Impact Engineering, 124*, 37-47.

18. Huang, G.-Y., Li, W., & Feng, S.-S. (2015). Axial distribution of Fragment Velocities from cylindrical casing under explosive loading. *International Journal of Impact Engineering, 76*, 20-27.

19. Li, Y., Yu, C., Suo, T., & Wen, Y. (2023). Maximum fragment velocity of hollow charges with different aspect ratios. *International Journal of Impact Engineering, 178*, 104622.

20. Li, W., Huang, G.-Y., & Feng, S.-S. (2015). Effect of eccentric edge initiation on the fragment velocity distribution of a cylindrical casing filled with charge. *International Journal of Impact Engineering, 80*, 107-115.